NANO LETTERS

Letter

pubs.acs.org/NanoLett

Self-Assembly of Octapod-Shaped Colloidal Nanocrystals into a Hexagonal Ballerina Network Embedded in a Thin Polymer Film

Milena P. Arciniegas,[†] Mee R. Kim,[†,⊥] Joost De Graaf,[‡] Rosaria Brescia,[†] Sergio Marras,[†] Karol Miszta,[†] Marjolein Dijkstra,[§] René van Roij,[∥] and Liberato Manna[†,*]

[†]Istituto Italiano di Tecnologia (IIT), via Morego 30, IT-16163 Genova, Italy

[‡]Institute for Computational Physics (ICP), University of Stuttgart, Allmandring 3, 70569 Stuttgart, Germany

[§]Soft Condensed Matter, Debye Institute for Nanomaterials Science, Utrecht University, Princetonplein 5, 3584 CC Utrecht, The Netherlands

[∥]Institute for Theoretical Physics, Utrecht University, Princetonplein 5, 3584 CE Utrecht, The Netherlands

S *Supporting Information*

ABSTRACT: Nanoparticles with unconventional shapes may exhibit different types of assembly architectures that depend critically on the environmental conditions under which they are formed. Here, we demonstrate how the presence of polymer (polymethyl methacrylate, PMMA) molecules in a solution, in which CdSe(core)/CdS(pods) octapods are initially dispersed, affects the octapod-polymer organization upon solvent evaporation. We show that a fast drop-drying process can induce a remarkable two-dimensional (2D) self-assembly of octapods at the polymer/air interface. In the resulting structure, each octapod is oriented like a "ballerina", that is, only one pod sticks out of the polymer film and is perpendicular to the polymer−air interface, while the opposite pod (with respect to the octapod's center) is fully immersed in the film and points toward the substrate, like a ballerina performing a grand battement. In some areas, a hexagonal-like pattern is formed by the ballerinas in which the six nonvertical pods, which are all embedded in the film, maintain a pod−pod parallel configuration with respect to neighboring particles. We hypothesize that the mechanism responsible for such a self-assembly is based on a fast adsorption of the octapods from bulk solution to the droplet/air interface during the early stages of solvent evaporation. At this interface, the octapods maintain enough rotational freedom to organize mutually in a pod−pod parallel configuration between neighboring octapods. As the solvent evaporates, the octapods form a ballerina-rich octapod-polymer composite in which the octapods are in close contact with the substrate. Finally, we found that the resulting octapod-polymer composite is less hydrophilic than the polymer-only film.

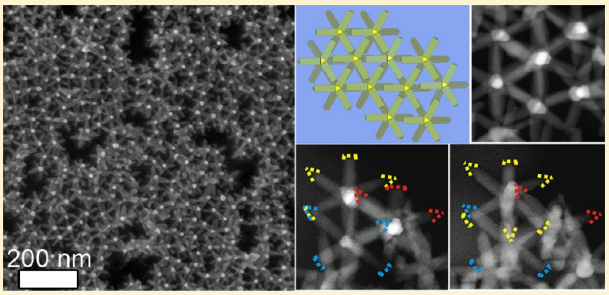

KEYWORDS: *Octapods, self-assembly, interface adsorption, polymer, nanocomposite*

Colloidal branched nanocrystals (bNCs) have attracted scientific attention in recent years due to their potential use as building blocks of complex and functional superstructures with possible applications in the fields of nano-optoelectronics, photonics, or plasmonics.[1−7] In contrast to isotropic nanocrystals, the self-organization of bNCs (especially those with long "branches") into ordered superstructures can be hindered by intricate couplings between the translational and rotational degrees of freedom at high volume fractions of nanocrystals (the typical conditions under which ordered assemblies of colloidal particles are formed) and can cause them to get kinetically trapped into disordered, amorphous structures. Also, the mutual interactions between nanocrystals with complex shapes can be dominated by anisotropic van der Waals (vdW) forces, the strength of which is influenced by various factors including the shape of the bNCs, the type of stabilizing molecules bound at their surface, the solvent, and the NC concentration.[8−11] This high dimensionality of the parameter space can be used to potentially realize many different assembly symmetries, depending on the experimental conditions under which assembly is attempted, yet at the same time it complicates explicit predictions. Nevertheless, for branched octapod-shaped nanocrystals (referred to as "octapods" in the remainder of this paper) we recently demonstrated a fine control over shape and size,[12,13] to the point that ordered superstructures of these nanocrystals have not only been experimentally observed but also theoretically explained by our groups.[14−16] In fact, we have shown that different configurations of self-assembled octapods can be achieved both in bulk solution and on flat substrates; see Schemes I and II in Figure 1, respectively.[14−16]

Received: December 20, 2013
Revised: January 15, 2014
Published: January 21, 2014

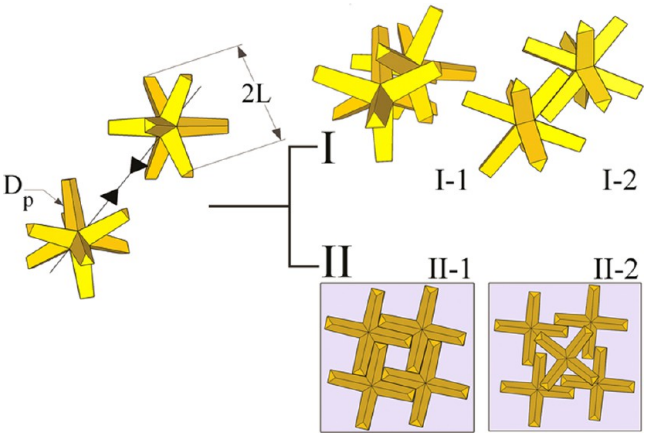

Figure 1. (Left) Sketch of two approaching octapods. For each octapod, the tip-to-tip length is $2L$, and the pod diameter is D_p. (Right) I. The two lowest energy configurations of an octapod–octapod dimer in bulk solution, as determined from theoretical calculations of the vdW interactions: (I-1) "interlocked" configuration and (I-2) pod–pod parallel configuration. Both configurations are involved in the experimentally observed formation of 3D octapod superstructures in solution.[14] II. The experimentally observed (and calculated) 2D configurations of octapods on a flat substrate after solvent evaporation:[16] Square-lattice (II-1) and binary square lattice (II-2).

In bulk solution, we experimentally demonstrated the formation of short linear chains of interlocked octapods (Scheme I-1 in Figure 1) through an aging process of an octapod-rich toluene solution. After the addition of acetonitrile longer linear chains were formed,[14] followed by the self-assembly of the chains into a porous three-dimensional (3D) superstructure with parallel pod–pod alignment (Scheme I-2 in Figure 1). Using theoretical calculations of the vdW interactions, we demonstrated that the interlocked and pod–pod parallel arrangements are energetically the most favorable configurations in bulk solution,[14] thus explaining the experimental observations.

On flat substrates, we demonstrated instead that ordered monolayers of octapods can be formed in a side-to-side configuration through solvent evaporation. The monolayers could consist either of simple or binary square lattices, depending on the aspect ratio L/D_p of the pods (see Scheme II-1 and II-2 in Figure 1).[15,16] In those experiments, both a fast solvent evaporation and the presence of the substrate limit the 3D rotation of the octapods and constrain the octapods to stand on four pods on the substrate, thereby preventing the formation of interlocked structures in the "coffee stain". To date, octapod superstructures have thus been obtained by exploiting either the more favorable interlocked configuration in solution, or the additional constraint imposed by the presence of a flat substrate.

Apparently, assemblies with the pod–pod parallel configuration (Scheme I-2 in Figure 1) are difficult to realize, most likely because they require a good balance between steric repulsion at short distances and vdW forces to cause the two octapods to approach each other along parallel axes.[14] This is far less likely to be achieved for single octapods in bulk solution, given their geometrical restrictions in addition to the steric/vdW balance requirement.[17] In order to achieve the parallel pod–pod configuration for octapods, long pods are preferred over short ones. The reason is that the increased contact area between longer pods in the pod–pod configuration causes stronger pod–pod vdW attractions, which can dominate over the core–core vdW attractions that stabilize the interlocked configuration. It should be noted that small-scale assemblies of tetrapodal branched NCs with parallel pod–pod configurations have already been reported. This type of organization was achieved both via the Langmuir–Blodgett technique and by exploiting attractive depletion forces in a surfactant-rich (or polymer-rich) solution of NCs.[18,19]

In this work, we demonstrate the formation of superstructures of octapods that fully exploit the parallel pod–pod configuration. Such an assembly was serendipitously discovered upon drying a solution of octapods and excess unwashed organics on a SiO_2 substrate at room temperature in a solvent-saturated atmosphere. Here, the excess organics, which stem from the synthesis, are impurities mainly consisting of free unbound surfactants and Cd-phosphate complexes. Scanning electron microscopy (SEM) analysis of the sample after evaporation evidenced a ringlike deposit on the substrate with a primarily hexagonal-like structure as discerned from the top view shown in Figure 2a.

Figure 2a, which was acquired with a low-angle backscattered electron detector (LABE), reveals that the edges of the hexagons are formed by six pairs of pods from neighboring octapods (some of the hexagons are framed in yellow in Figure 2a to illustrate this). For each octapod belonging to this superstructure, only one tip was observed when the same zone was scanned with an upper secondary electron detector (SEI), see Figure 2b. This image shows a strong contrast between the octapods (bright posts) and the organic film (light gray); see also a top view of the structure in the Supporting Information Figure S1a,b. A SEM image of the same zone, using a lower secondary electron detector (LEI), Figure 2c, demonstrates that the octapods are standing upright with one pod on the substrate (see the inset), in what we refer to as a "ballerina" configuration forming the hexagonal network (see sketches in Figure 2d).

Starting from this point, we intentionally prepared mixtures of octapods with a conventional polymer (polymethyl methacrylate, PMMA) in order to improve the control over the self-assembly process into this "ballet of nanoballerinas". For this purpose, we first washed the octapods several times to remove the excess of organics that derived from the synthesis. This cleaning was also useful to improve the dispersion of octapods in the polymer solutions and to ensure a more direct contact with the polymer. As screening experiments, we mixed solutions of PMMA and octapods in toluene at different concentrations to estimate the solubility threshold using (i) the turbidity of the solution as a first sign of aggregation, and (ii) dynamic light scattering measurements to assess the size of aggregates after the addition of the polymer. We also varied the molecular weight of the polymer, M_w, in these experiments, see Supporting Information Figure S2. We found that polymer concentrations above 5% vol induced visible aggregation of octapods in PMMA solutions, especially for high M_w. Therefore, the concentration of PMMA (with M_w = 120 000 g/mol) was maintained far below 5% vol in the subsequent experiments. This ensures a large number of well-dispersed octapods in the toluene-PMMA solution, right before the toluene evaporation and the film formation. Also the concentration of octapods in the composite solution was found to play an important role, since large-scale self-assembly requires a sufficiently high initial concentration. For an octapod

dx.doi.org/10.1021/nl404732m | Nano Lett. 2014, 14, 1056–1063

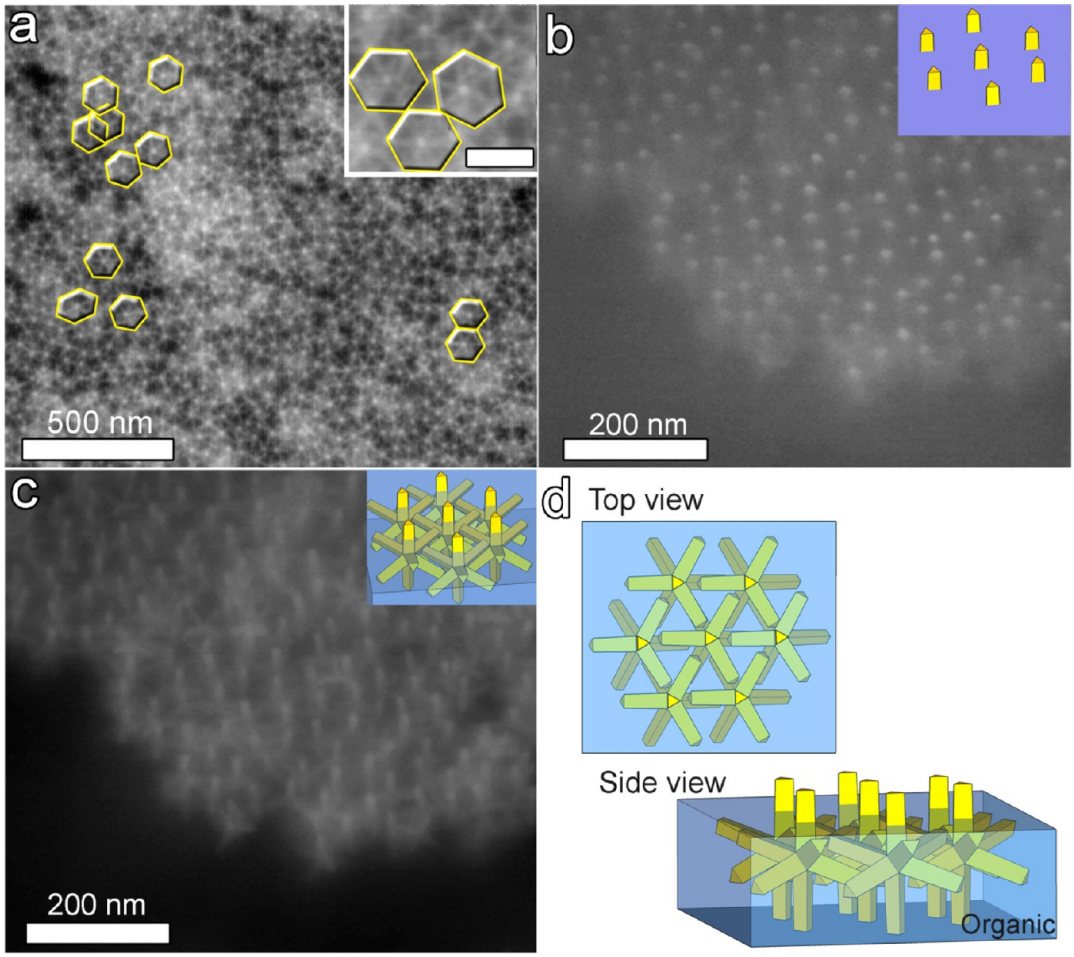

Figure 2. Arrangement of octapods after slow drying of a drop from an organic-rich toluene solution. (a) LABE-SEM top-view image revealing the self-assembly of octapods into a hexagonal-like structure in the coffee-stain region formed on the SiO_2 substrate; the inset shows a close-up view of the same image. (b) A 45°-tilt-SEI-SEM image demonstrating the presence of the organic residues (light gray); for each octapod only the upper section of the pod pointing upward actually protrudes out of the organic film (see sketch in the inset). (c) A 45°-tilt-LEI-SEM image of the same zone evidencing that the remaining seven pods are inside the organic layer (see sketch in the inset). (d) Sketches summarizing the observed assembly in both top and side view.

concentration below 10^{-7} M only small-scale structures were formed independent of the PMMA concentration (see Supporting Information Figure S3a).

In another series of experiments, drops from repeatedly washed octapod solutions with no added polymer, as well as drops from octapod-polymer mixtures, were cast on carbon-coated Cu grids for transmission electron microscopy (TEM) and on a 10 nm carbon-coated SiO_2 wafer. Both types of substrate have poor hydrophilic character, which should help to avoid ringlike deposits. The solvent was allowed to evaporate in air (yielding a faster evaporation rate) at room temperature (25 °C) and relative humidity of 55%. When polymer-free octapod solutions were drop-cast, we found after sufficiently fast evaporation that the octapods had four pods in contact with the substrate (see Figure 3a and Supporting Information Figure S1d). These octapods formed short-ranged 2D-ordered structures in some areas, depicted by the sketch in Figure 3a, similar to the square-lattice configuration reported by us in a previous work.[16] However, for sufficiently slow evaporation we found for the same polymer-free octapod solution mainly interlocked chain-like assemblies, similar to those reported in another one of our papers[14] (see Supporting Information Figure S1c). This exemplifies the key role of the excess organic residues in the self-assembly of the ballerina configuration.

A remarkably different self-assembled network of octapods was obtained after adding PMMA at 1% vol to the NC solution (1:4 volume ratio of octapod/PMMA solution). Drop-casting the octapod-polymer mixture and evaporating the solvent (see Figure 3b) yielded a network of octapods with a primarily hexagonal-like structure, as evidenced in the inset in Figure 3b. Also, the octapods in this configuration were partially immersed in the PMMA layer (which appears as the intermediate gray level in Figure 3c). The thickness of the PMMA layer embedding the ballerina assemblies on the C-support film on the TEM grid was estimated to be 71 ± 7 nm by evaluating the inelastic scattering undergone by electrons in the TEM (log-ratio method, see Supporting Information);[20] this thickness is about 73% of the tip-to-tip distance $2L$ of an octapod (see the left sketch of Figure 1). A tilted SEM image of the structure demonstrated that the octapods have one pod sticking out of the polymer/air interface (bright posts in Figure 3d), forming the ballerina configuration in the PMMA.

Detailed SEM observation of samples from which the polymer was removed by an oxygen plasma treatment confirmed that the ballerina-hexagonal arrangement of the

dx.doi.org/10.1021/nl404732m | Nano Lett. 2014, 14, 1056−1063

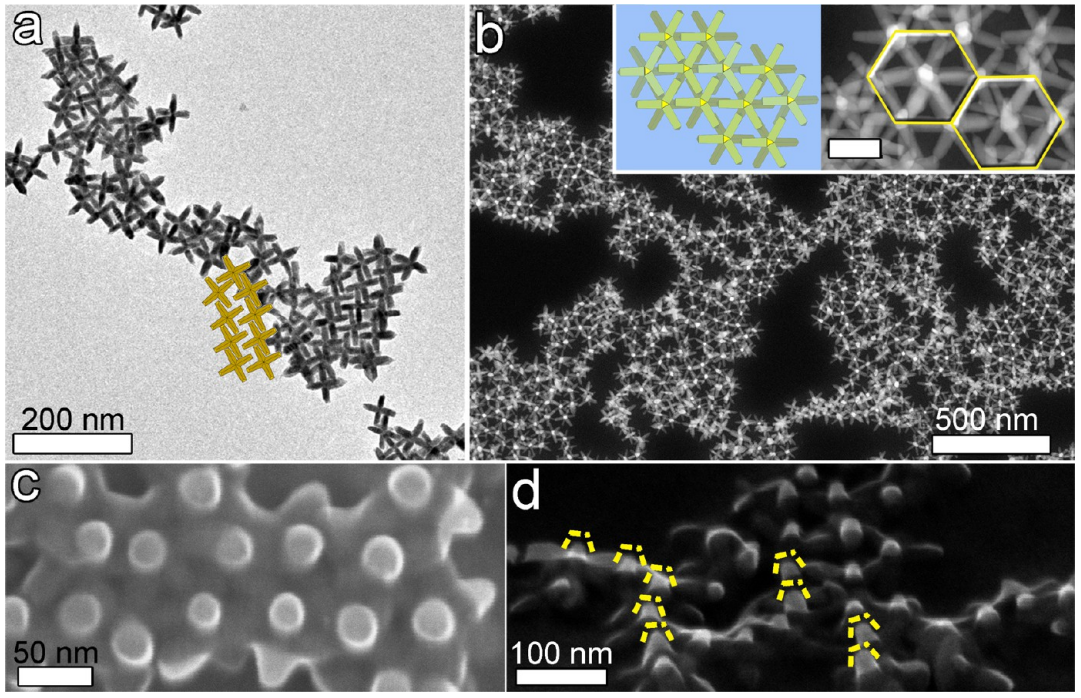

Figure 3. (a) TEM image of the repeatedly washed toluene suspension with octapods after fast solvent evaporation. The particles are touching the substrate (carbon support film on Cu grid for TEM) with four pods. Most of the octapods formed a short-ranged square-lattice-like structure. The cartoon embedded in the figure highlights the octapod pattern. (b) HAADF-STEM image showing the self-assembled ballerina network of octapods formed after drop-casting of PMMA-octapod solutions (PMMA at 1% vol) and fast solvent evaporation; the insets evidence the locally regular hexagonal-like structure. Scale bar: 50 nm. (c) Top-view SEM image of the sample in (b) that confirms the ballerina configuration, also showing that the octapods are partially embedded in the polymer. (d) A 45°-tilt-SEM image in which the single protruding pod from each of the embedded octapods can be discerned (framed in yellow dashed lines).

octapods consisted of one single layer on the substrate (see Figure 4a). This arrangement was further confirmed by HAADF- STEM images taken at different tilt angles (see Figure 4b, Supporting Information Figure S4 and movie SI1.avi and SI2.avi). The pod−pod parallel configuration of neighboring octapods is indeed consistent with the hexagonal-like arrangements of the bright posts viewed in SEM (Figure 2) and in HAADF-STEM plan-view images (Figure 3b).

This superstructure formation is reminiscent of the self-assembly of NCs induced by liquid/air interface techniques, which result in uniform distributions of NCs at the interface under equilibrium conditions.[18,21−24] Unlike controlled solvent evaporation, which given enough time is in favor of 3D ordered structures, fast solvent evaporation forces the nanoparticles out of equilibrium and may drive the system toward a different self-assembled state.[25−27] The formation of the ballerina network must be a consequence of the addition of the PMMA to the octapod solution, because in the absence of the PMMA no ordered domains with the ballerina configuration were observed. Moreover, we note that the observed hexagonal-like arrangements of ballerina octapods are not densely packed, which indicates that the forces exerted during drying are insufficient to drive the octapods to their optimal packing, in contrast with the results obtained for drop-cast, slow-dried solutions of octapods without PMMA added.[15,16] This suggests that forces other than those caused by drying play a dominant role during the later stages of the self-assembly. Hence we hypothesize that the octapods reach the observed ballerina configuration in the following three stages:

- Stage I (Figure 4c-I): immediately after drop deposition, the octapods are free to diffuse through the toluene-PMMA medium, as the viscosity of the solution is still low. The fast evaporation of the toluene, however, tends to force the octapods to the droplet−air interface. This process can be explained by considering the octapod diffusion coefficient D in the solution. The octapod diffusion is time-dependent due to the changes in the viscosity η of the medium during drying, as can be seen from the Stokes−Einstein equation for nanoparticles with a hydrodynamic radius r, given by $D = k_B T/6\pi\eta r$ with k_B as the Boltzmann constant and T as the temperature. Because of the increase in the viscosity of the PMMA-solution during the toluene evaporation, the diffusion of the octapods D decreases significantly. This causes the octapod movement to eventually become slower than the advancement rate of the polymer−air interface, thereby forcing the octapods to the interface.
- Stage II (Figure 4c-II): at the interface, the free energy of adsorption causes the octapods to adopt a specific, albeit yet unknown, orientation. It should be noted that the vertical constraint provided by the interfacial energy that forces the octapods to remain trapped at the interface does not hinder its lateral movements. In this stage, as reported in other works on interfacial self-assembly,[28−32] the adsorption of the octapods at the interface could induce the formation of a capillary multipole structure around the NCs. The multipolar octapod−octapod capillary interactions may then facilitate the octapods coming together in a specific way. For instance, the octapods could approach each other with their pods almost aligned, leading the way for interactions that dominate the multipolar component at short ranges to take over, causing the already prealigned octapods to self-assemble into a pod−pod ballerina network. However, it is equally possible that the droplet shrinking due to

dx.doi.org/10.1021/nl404732m | Nano Lett. 2014, 14, 1056−1063

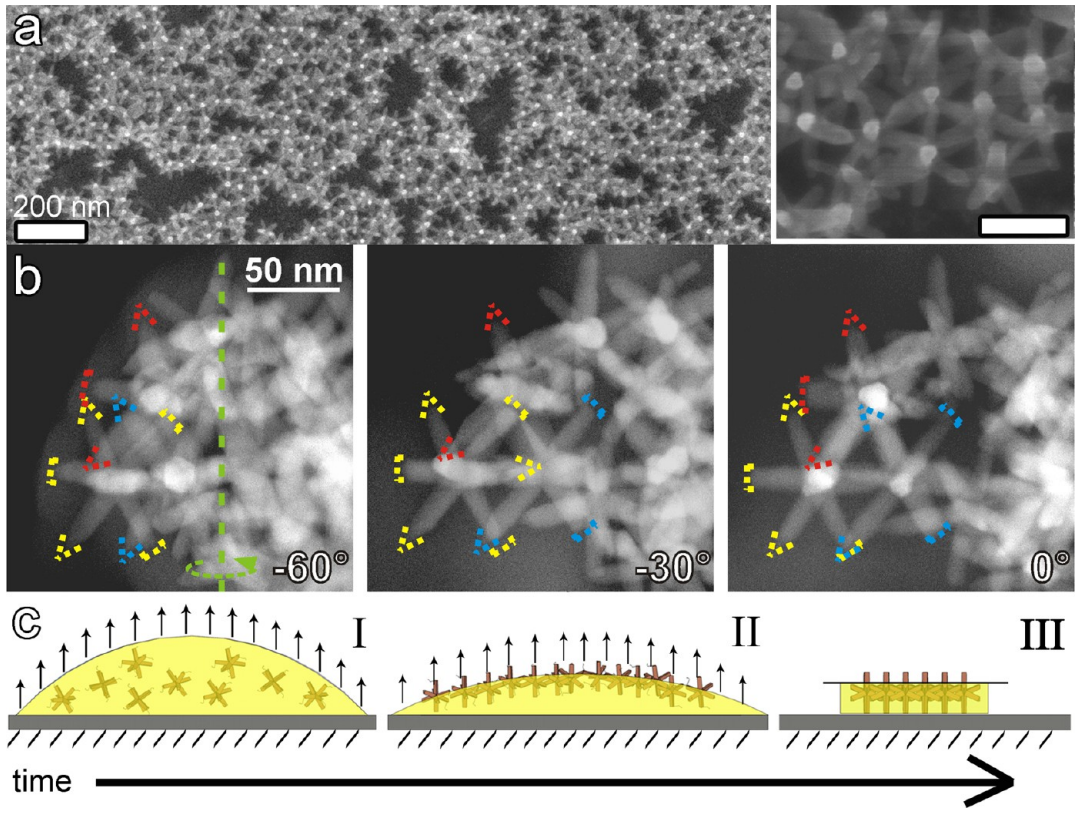

Figure 4. (a) SEI-SEM image after removing the polymer (via an oxygen plasma treatment) evidencing that the ballerinas are standing on the substrate. The inset shows a close-up view of an ordered domain. The scale bar is 60 nm. (b) HAADF-STEM images at different tilt angles confirming the pod−pod parallel arrangement between octapods forming the hexagonal array of ballerinas. (c) Cartoon explaining the formation of the ballerinas at the droplet/air interface. (I). The particles are constrained to move toward the interface and remain trapped there during drying; weak vdW and interfacial interactions are responsible for the pod−pod configuration (II−III).

fluid evaporation is the dominant term in the drying forces that cause the octapods to be driven together. Moreover, capillary attractions and interfacial deformation could only play a subdominant role in the formation of the ballerina network. In this scenario, the final step of the self-assembly might then be entirely caused by other effects, such as substrate-mediated orientational ordering. We therefore conjecture that in Stage II the octapods are driven together by a combination of droplet shrinking and capillary attraction, both of which may dominate the aggregation of the octapods at different points during the drying.

- Stage III (Figure 4c-III): when the octapods are in mutual close proximity, they start to interact presumably mostly through vdW forces, since the ballerina network shows pod−pod configurations. Drying and adsorption free energies are apparently sufficiently slow and low, respectively, to allow the octapods to reorient from their adsorbed orientation to one where they form pod−pod parallel arrangements with their neighbors (see the inset in Figure 4a and Figure 4b), rather than be forced together into a densely packed state. As mentioned in the description of Stage II, the reorientation may be induced by multipolar interactions stemming from the deformation of the interface, but could equally well be caused by a host of other forces, including restrictions imposed by the substrate.

In our description of the various stages, we stated that interfacial adsorption could play a significant role in the self-assembly mechanism, since it might favor a configuration that facilitates octapods forming pod−pod contacts through vdW forces rather than interlocked or dense-packed configurations; the interfacial adsorption may even prevent the formation of interlocked contacts via a free-energy penalty. Therefore, we calculated the adsorption free energy for the octapod/polymer system (see Supporting Information for additional details) in order to gauge the relevance of adsorption on the formation of the ballerina configuration. Similar calculations have proven their usefulness in clarifying the adsorption of nanoparticles at fluid interfaces and the self-assembled structured that these particles formed.[21] In our calculations, we considered the optimal adhesion at a flat nondeformable toluene−air interface for a single octapod as a function of the (cosine of the) contact angle ($\cos\theta$ in Figure 5) between the octapod material and the solvent interface,[33,34] as the system's wettability depends on the solvent (with polymer)−octapod, air−octapod, and solvent−air

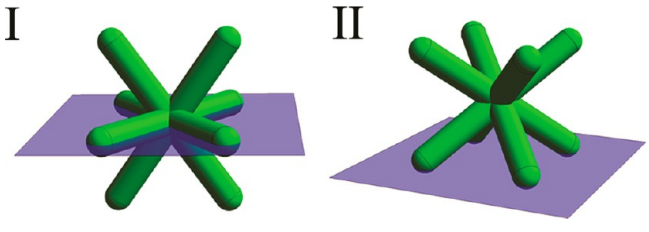

Figure 5. The archetypical configurations for an octapod adsorbed at a flat nondeformable interface between air (below) and toluene/polymer (above) for a cosine of the contact angle in the range (I) $0.0 \leq \cos\theta \leq 0.3$ and (II) $0.3 < \cos\theta \leq 0.9$; the octapod is fully detached for $\cos\theta > 0.9$.

dx.doi.org/10.1021/nl404732m | *Nano Lett.* 2014, 14, 1056−1063

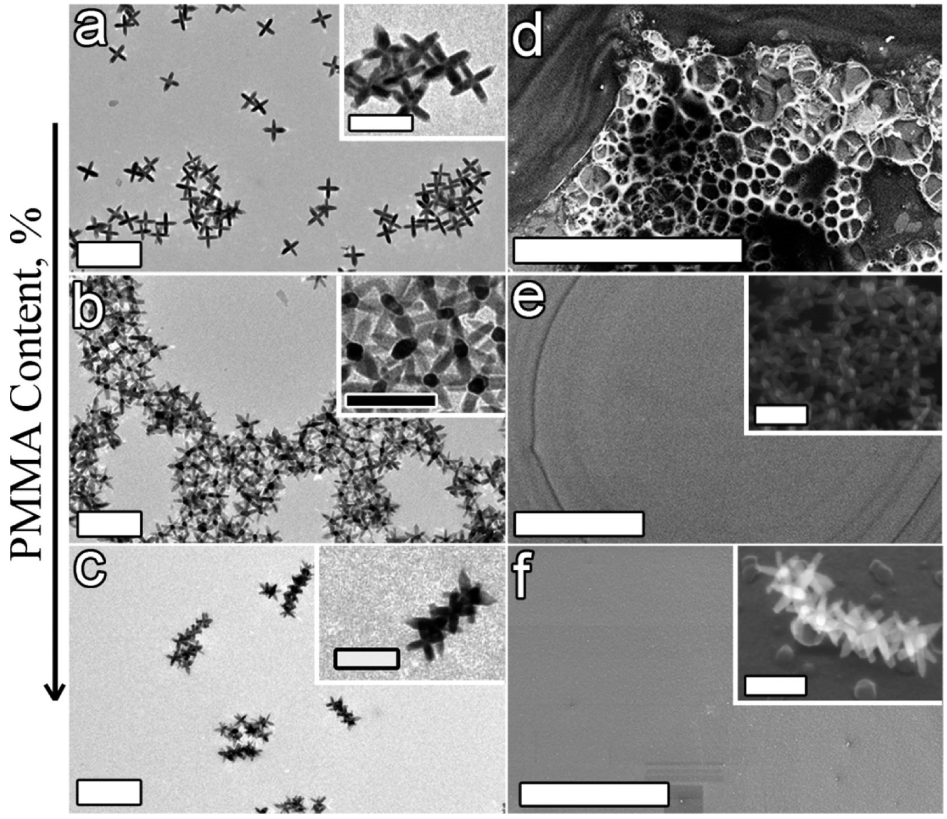

Figure 6. (a–c) TEM images of the PMMA-based nanocomposite revealing how octapod configurations depend on the polymer content/thickness. (a) Octapods standing on four-pods touching the substrate with an evident strong dewetting of the polymer (PMMA 0.5% vol.) on the substrate as can be seen in panel d; scale bar: 200 nm. (b) Octapods in the ballerina configuration (PMMA 1.0% vol.). (c) Interlocked octapods forming short chains (PMMA 5.0% vol.); the insets show a close-up view of each arrangement; scale bar: 50 nm. (d–f) SEM images evidence the morphology of the films depending on the polymer content; scale bars: 200 nm. Strong dewetting for more diluted solutions (d) and a more uniform and thicker film from concentrated PMMA solutions loaded with octapods (e,f). The insets show a 30°-tilt-SEM image of the ballerina configuration and the chainlike interlocked octapods after removal of the polymer by oxygen plasma treatment.

surface tensions. We also limited ourselves to a single contact angle all over the octapod surface, thereby ignoring possible chemical and structural heterogeneities to avoid further complications in the analysis. However, even such a simple model can give insights into the behavior of bNCs at an interface. Our results suggest that the octapod's orientation and trapping at the interface can be strongly influenced by the wettability of the particles. However, they also show that the cause of the experimental observations is not to be sought solely in an adsorption mechanism, as neither of the orientations of octapods obtained here corresponds to the ballerina configuration (see Supporting Information Figure S4). We found instead two optimal trapping configurations, as shown in Figure 5, for which the octapods are partially wetted by the polymer solution: (I) four-arms lie flat on the interface and two stick out on either side and (II) the octapod rests on the interface with four tips slightly penetrating it. We refer to these configurations as archetypical, because over the range of contact angles that we considered there are only slight variations in the exact position and orientation of the octapod at the interface with respect to these two configurations (see Supporting Information Figure S4). However, there is a very sharp transition from configuration I to configuration II, with no intermediate states.

Our result can be explained by the way the system minimizes its free energy. When there is little difference between the media ($\cos\theta$ is small) the octapod excludes the maximum surface area from the interface, while when the difference between the media is large ($\cos\theta$ is large) the octapod minimizes its contact with the energetically unfavored medium. This is true in general, since the free energy of adsorption can be lowered by removing part of the interface, but strongly hydrophobic/hydrophilic colloids would still prefer to minimize their contact with the unfavored medium.[21] Note that neither of the archetypical configurations corresponds to the observed ballerina configuration. We therefore conjecture that the ballerina configuration is unlikely to be explained by adsorption to the interface alone, since the ballerina configuration itself does not exclude a particularly big part of the interface, nor does it seem to minimize contact with the air. Moreover, adding a polymer, which changes the contact angle properties of the system, is unlikely to prevent the octapods from being driven toward their dense-packed configuration in an adsorption-only self-assembly scenario. It is, however, possible that when the octapods are in close proximity the deformation of the interface aids in the formation of the ballerina network. The final state is likely achieved by the interplay between various effects, such as, adsorption, vdW forces, restrictions imposed by the substrate, and the slowing of the dynamics in the final stage of the self-assembly brought on by the increased viscosity of the solution.

Because the polymer content is known to strongly influence the adsorption properties, we considered the assemblies that formed upon varying the polymer content. We found different

dx.doi.org/10.1021/nl404732m | *Nano Lett.* 2014, 14, 1056–1063

octapod configurations in the PMMA film when the amount of polymer injected into the octapod solution was increased from 0.5 to 5% vol. (see Figure 6a–c). Octapods with four pods in contact with the substrate were observed for a PMMA concentration between 0 and 0.5% vol. A sharp change in the self-assembly behavior was observed when the PMMA concentration was increased up to 5.0% vol since ballerinas formed at 1% vol as we have seen already, and interlocked chains of 5–8 octapods were found in these films at 5% vol. This remarkable variation in configurations by changing the PMMA content is attributed to an increase in the number of polymer molecules wrapping the octapod surface, which can further lead to the formation of well-ordered aggregates by stronger octapod–octapod interactions.[35−37] These conditions, however, are not in favor of the ballerina configuration, as both the viscosity of the solution and the thickness of the final film are increased with an increasing PMMA content. In this case, because the diffusion coefficient D of the octapods is drastically decreased, the movement of the octapods is limited and they are forced to remain embedded in the polymer film until the end of the solvent evaporation.

Our observations by SEM of the samples prepared on carbon-coated SiO_2 substrates revealed a strong dewetting of the polymer film on the substrate in the case of a more diluted PMMA solution (see Figure 6d), whereas samples containing larger amounts of PMMA resulted in more homogeneous films (see Figure 6e,f) because of the lower fluidity of the polymer. We observed a higher shrinkage of the polymer in the center area in the sample containing 1% of PMMA (see Figure 6e), which we attributed to the solvent evaporation rate. Measurements of the thickness of these films conducted by a nanoprofilometer indicated a variation from the center area to the edges of the drop spreading from about 68 to 100 nm and from 230 to 300 nm for 1 and 5% of PMMA, respectively. Removal of the polymer revealed that the ballerina configuration was obtained in the 1% PMMA film (see inset in Figure 6e) in the area with a thickness of ∼70 nm, while interlocked octapods were observed for 5% PMMA content (see inset in Figure 6f).

In order to further study the impact of the ballerina network on the surface properties of the PMMA composite film, we evaluated how this configuration affects the contact angle of water wetting the film. Contact angle measurements were performed using the sessile-drop method with ultrapure water (see the Supporting Information for details). Figure 7 shows the mean contact angle determined on the octapod-PMMA thin film deposited on carbon-coated SiO_2 substrates. Both a SiO_2 and a PMMA thin film on a carbon coated SiO_2 substrate were used as control materials.

The octapod/PMMA substrate gives rise to a significantly higher value of the contact angle than the references; after the formation of the ballerina network islands on the PMMA film, the contact angle increased significantly, that is, by more than 10° from 71.5 to 85.3°. This is attributed to the effect of the pod protruding from the polymer layer that is formed during the last stage of the evaporation in the thinner area of the film. Because of a variation in the polymer flow, the local roughness of the film may also be increased, thereby helping to pin the drop of water and inducing a more hydrophobic character in the hydrophilic PMMA.

In summary, we have presented a new assembly of octapod-shaped nanocrystals formed via fast drop casting of a PMMA/toluene/octapod solution on a flat substrate. The networks that we observed consist of octapods partially immersed in a thin polymer film. These octapods stand on the substrate with one pod oriented perpendicular to the substrate, while the opposing pod slightly penetrates the polymer/air interface. Neighboring ballerina octapods have a parallel pod–pod arrangement between the remaining six pods that causes them to form a hexagonal-like lattice. We have studied how the octapod self-assembly changes with the increase in polymer content from the formation of nonordered aggregates at low polymer concentration to the formation of ordered hexagonal ballerinas or short linear chains at higher polymer concentrations. We relate this to an increased probability of attractive pod–pod interactions. We hypothesize that upon increasing the PMMA content, the adsorption of octapods at the interface, in combination with van der Waals interactions between the octapods, and the restrictions imposed by the substrate, are the key parameters that control the formation of the ballerina configuration. These ingredients might all play an important role during the different regimes of solvent evaporation of a viscous solution, where a droplet spreads and dries on a wettable substrate. We have demonstrated that the ballerina octapod-polymer composite has an enhanced hydrophobicity with respect to that of a pure polymer film. Better understanding of the key parameters involved in the formation of this unusual network will be the subject of follow-up studies, which may provide indications for the scaling-up of the process and the optimization of this structure, leading to its potential use in nanodevices. For instance, achieving a ballerina network in a polymer thin film may improve its structural and mechanical stability, as it might work as nanopinned network to impede crack propagation.

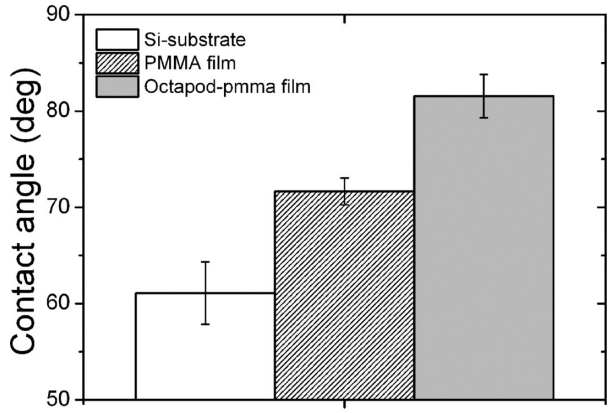

Figure 7. Contact angle with (ultrapure) water determined for the ballerina network on the PMMA film revealing loss of the hydrophilic character of the PMMA film attributed to the presence of the nanopinned surface formed by the octapods.

■ ASSOCIATED CONTENT

Ⓢ Supporting Information

Additional information, figures, and videos. This material is available free of charge via the Internet at http://pubs.acs.org.

■ AUTHOR INFORMATION

Corresponding Author

*E-mail: liberato.manna@iit.it.

Present Address

[⊥]Institut National de la Recherche Scientifique (INRS), Université du Québec, 1650 Boulevard Lionel-Boulet, Varennes, Québec, J3X 1S2 Canada.

Author Contributions

The manuscript was written through contributions of all authors. All authors have given approval to the final version of the manuscript.

Notes

The authors declare no competing financial interest.

■ ACKNOWLEDGMENTS

M.P.A., M.R.K., R.B., S.M., K.M., and L.M. acknowledge financial support from European Union through the FP7 starting ERC Grant NANO-ARCH (Contract Number 240111). J.D.G. acknowledges financial support from the NWO Rubicon Grant (680501210). Both R.v.R. and M.D. acknowledge financial support from an NWO-VICI grant. The authors would like to thank Dr. F. De Angelis, Dr. V. Lesnyak, and Dr. L. Ceseracciu for fruitful discussions.

■ REFERENCES

(1) Li, H.; Kanaras, A. G.; Manna, L. *Acc. Chem. Res.* **2013**, *46*, 1387−1396.
(2) Lim, B.; Xia, Y. *Angew. Chem., Int. Ed.* **2011**, *50*, 76−85.
(3) Das, P.; Kedia, A.; Kumar, P. S.; Large, N.; Chini, T. K. *Nanotechnology* **2013**, *24*, 405704.
(4) DeSantis, C. J.; Skrabalak, S. E. *Langmuir* **2012**, *28*, 9055−9062.
(5) Fu, X.-L.; Peng, Z.-J.; Li, D.; Zhang, L.; Xiao, J.-H.; Li, J.-Y.; Fang, Z.-Y. *Nanotechnology* **2011**, *22*, 175601.
(6) Manna, L.; Milliron, D. J.; Meisel, A.; Scher, E. C.; Alivisatos, A. P. *Nat. Mater.* **2003**, *2*, 382−385.
(7) Schulz, K. M.; Abb, S.; Fernandes, R.; Abb, M.; Kanaras, A. G.; Muskens, O. L. *Langmuir* **2012**, *28*, 8874−8880.
(8) Bishop, K. J. M.; Wilmer, C. E.; Soh, S.; Grzybowski, B. A. *Small* **2009**, *5*, 1600−1630.
(9) Mann, S. *Nat. Mater.* **2009**, *8*, 781−792.
(10) Min, Y.; Akbulut, M.; Kristiansen, K.; Golan, Y.; Israelachvili, J. *Nat. Mater.* **2008**, *7*, 527−538.
(11) Nie, Z.; Petukhova, A.; Kumacheva, E. *Nat. Nanotechnol.* **2010**, *5*, 15−25.
(12) Deka, S.; Miszta, K.; Dorfs, D.; Genovese, A.; Bertoni, G.; Manna, L. *Nano Lett.* **2010**, *10*, 3770−3776.
(13) Kim, M. R.; Miszta, K.; Povia, M.; Brescia, R.; Christodoulou, S.; Prato, M.; Marras, S.; Manna, L. *ACS Nano* **2012**, *6*, 11088−11096.
(14) Miszta, K.; de Graaf, J.; Bertoni, G.; Dorfs, D.; Brescia, R.; Marras, S.; Ceseracciu, L.; Cingolani, R.; van Roij, R.; Dijkstra, M.; Manna, L. *Nat. Mater.* **2011**, *10*, 872−876.
(15) Qi, W.; de Graaf, J.; Qiao, F.; Marras, S.; Manna, L.; Dijkstra, M. *J. Chem. Phys.* **2013**, *138*, 154504−1−154504−13.
(16) Qi, W.; Graaf, J. d.; Qiao, F.; Marras, S.; Manna, L.; Dijkstra, M. *Nano Lett.* **2012**, *12*, 5299−5303.
(17) de Graaf, J.; van Roij, R.; Dijkstra, M. *Phys. Rev. Lett.* **2011**, *107*, 155501.
(18) Goodman, M. D.; Zhao, L.; DeRocher, K. A.; Wang, J.; Mallapragada, S. K.; Lin, Z. *ACS Nano* **2010**, *4*, 2043−2050.
(19) Zanella, M.; Bertoni, G.; Franchini, I. R.; Brescia, R.; Baranov, D.; Manna, L. *Chem. Commun.* **2011**, *47*, 203−205.
(20) Egerton, R. F. *Electron Energy-Loss Spectroscopy in the Electron Microscope*, 3rd. ed.; Springer: New York, 2011.
(21) Evers, W. H.; Goris, B.; Bals, S.; Casavola, M.; de Graaf, J.; Roij, R. v.; Dijkstra, M.; Vanmaekelbergh, D. *Nano Lett.* **2012**, *13*, 2317−2323.
(22) Korgel, B. A. *Nat. Mater.* **2010**, *9*, 701−703.
(23) Modestino, M. A.; Chan, E. R.; Hexemer, A.; Urban, J. J.; Segalman, R. A. *Macromolecules* **2011**, *44*, 7364−7371.
(24) Xiong, S.; Dunphy, D. R.; Wilkinson, D. C.; Jiang, Z.; Strzalka, J.; Wang, J.; Su, Y.; de Pablo, J. J.; Brinker, C. J. *Nano Lett.* **2013**, *13*, 1041−1046.
(25) Bigioni, T. P.; Lin, X.-M.; Nguyen, T. T.; Corwin, E. I.; Witten, T. A.; Jaeger, H. M. *Nat. Mater.* **2006**, *5*, 265−270.
(26) Maki, K. L.; Kumar, S. *Langmuir* **2011**, *27*, 11347−11363.
(27) Rabani, E.; Reichman, D. R.; Geissler, P. L.; Brus, L. E. *Nature* **2003**, *426*, 271−274.
(28) Park, J.; Zheng, H.; Lee, W. C.; Geissler, P. L.; Rabani, E.; Alivisatos, A. P. *ACS Nano* **2012**, *6*, 2078−2085.
(29) Rabideau, B. D.; Pell, L. E.; Bonnecaze, R. T.; Korgel, B. A. *Langmuir* **2006**, *23*, 1270−1274.
(30) Oliver, S. R. J.; Bowden, N.; Whitesides, G. M. *J. Colloid Interface Sci.* **2000**, *224*, 425−428.
(31) Bowden, N.; Choi, I. S.; Grzybowski, B. A.; Whitesides, G. M. *J. Am. Chem. Soc.* **1999**, *121*, 5373−5391.
(32) Bowden, N.; Oliver, S. R. J.; Whitesides, G. M. *J. Phys. Chem. B* **2000**, *104*, 2714−2724.
(33) de Graaf, J.; Dijkstra, M.; van Roij, R. *J. Chem. Phys.* **2010**, *132*, 164902−1−164902−14.
(34) de Graaf, J.; Dijkstra, M.; van Roij, R. *Phys. Rev. E.* **2009**, *80*, 051405−1−051405−19.
(35) Hu, S.-W.; Sheng, Y.-J.; Tsao, H.-K. *J. Phys. Chem. C.* **2011**, *116*, 1789−1797.
(36) Rozenberg, B. A.; Tenne, R. *Prog. Polym. Sci.* **2008**, *33*, 40−112.
(37) Shenhar, R.; Norsten, T. B.; Rotello, V. M. *Adv. Mater.* **2005**, *17*, 657−669.